ASME Journal of Biomechanical Engineering
Online journal at:
https://asmedigitalcollection.asme.org/biomechanical

Differences in Glenohumeral Joint Contact Forces Between Recovery Hand Patterns During Wheelchair Propulsion With and Without Shoulder Muscle Weakness: A Simulation Study

Shelby L. Walford
Walker Department of Mechanical Engineering,
The University of Texas at Austin,
Austin, TX 78712-1591

Jeffery W. Rankin
Pathokinesiology Laboratory,
Rancho Los Amigos
National Rehabilitation Center,
Downey, CA 90242;
Rehabilitation Engineering,
Rancho Los Amigos
National Rehabilitation Center,
Downey, CA 90242

Sara J. Mulroy
Pathokinesiology Laboratory,
Rancho Los Amigos
National Rehabilitation Center,
Downey, CA 90242;
Rehabilitation Engineering,
Rancho Los Amigos
National Rehabilitation Center,
Downey, CA 90242

Richard R. Neptune[1,2]
Walker Department of Mechanical Engineering,
The University of Texas at Austin,
Austin, TX 78712-1591
e-mail: rneptune@mail.utexas.edu

The majority of manual wheelchair users (MWCU) develop shoulder pain or injuries, which is often caused by impingement. Because propulsion mechanics are influenced by the recovery hand pattern used, the pattern may affect shoulder loading and susceptibility to injury. Shoulder muscle weakness is also correlated with shoulder pain, but how shoulder loading changes with specific muscle group weakness is unknown. Musculoskeletal modeling and simulation were used to compare glenohumeral joint contact forces (GJCFs) across hand patterns and determine how GJCFs vary when primary shoulder muscle groups are weakened. Experimental data were analyzed to classify individuals into four hand pattern groups. A representative musculoskeletal model was then developed for each group and simulations generated to portray baseline strength and six muscle weakness conditions. Three-dimensional GJCF peaks and impulses were compared across hand patterns and muscle weakness conditions. The semicircular pattern consistently had lower shear (anterior-posterior and superior-inferior) GJCFs compared to other patterns. The double-loop pattern had the highest superior GJCFs, while the single-loop pattern had the highest anterior and posterior GJCFs. These results suggest that using the semicircular pattern may be less susceptible to shoulder injuries such as subacromial impingement. Weakening the internal rotators and external rotators resulted in the greatest increases in shear GJCFs and decreases in compressive GJCF, likely due to decreased force from rotator cuff muscles. These findings suggest that strengthening specific muscle groups, especially the rotator cuff, is critical for decreasing the risk of shoulder overuse injuries. [DOI: 10.1115/1.4064590]

Keywords: rehabilitation, biomechanics, shoulder pain, modeling and simulation

1 Introduction

The majority of MWCU develop shoulder pain or injuries [1], with impingement of the subacromial structures [2] and rotator cuff tears [3] being common causes of shoulder pain. To prevent shoulder pain and injuries, current clinical recommendations are to have MWCU adopt propulsion techniques that decrease cadence, increase the arc of contact with the pushrim (i.e., contact angle), and increase contact time as a percentage of the propulsion cycle [4,5]. The trajectory of the hand during the propulsion cycle (i.e., hand pattern, Fig. 1) influences the propulsion mechanics. For example, the semicircular (SC) pattern is typically associated with decreased cadence, increased contact angle [4–6], and decreased joint accelerations [7], suggesting that it is a more favorable pattern to use [8]. The double-loop (DL) pattern has also been associated with lower cadence [5] and more effective (i.e., more tangentially directed) handrim forces, similar to SC [9]. While the arcing (ARC) and single-loop (SL) patterns are typically not recommended due to increased cadence and decreased contact angles [5], recent work found no difference between the SC and ARC patterns in supraspinatus compression risk that may lead to joint pain [10]. Another study found that using the SL pattern during fast wheelchair propulsion did not correlate with shoulder pain development [11]. Recent work also found that SL had a smaller decrease in supraspinatus and biceps tendon thickness right after propulsion compared to the other patterns, suggesting that using SL is less likely to result in strain or injury to these tendons [12]. Thus, further analyses are needed to understand how differences associated with each hand pattern influence the susceptibility of the shoulder joint to pain and injury.

Musculoskeletal modeling and simulation are useful tools for estimating joint loading and muscle forces. Previous modeling and simulation work analyzing wheelchair propulsion has provided insight into the role of the shoulder muscles during push and

[1]Present Address: Walker Department of Mechanical Engineering, The University of Texas at Austin, 204 E. Dean Keeton Street, Stop C2200, Austin, TX 78712-1591.
[2]Corresponding author.
Manuscript received May 8, 2023; final manuscript received January 16, 2024; published online February 23, 2024. Assoc. Editor: Angela E. Kedgley.

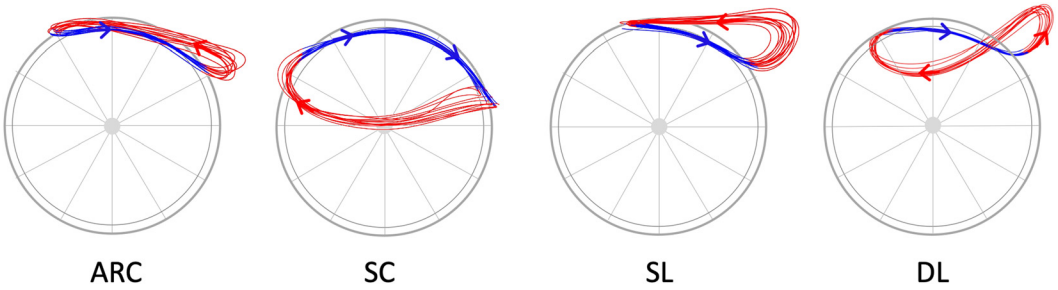

Fig. 1 Four commonly used hand patterns: arcing (ARC), semicircular (SC), single-loop (SL), and double-loop (DL) observed during manual wheelchair propulsion. Arrows represent the direction of the hand's motion during the push and recovery phases.

recovery [13,14], shoulder muscle forces and joint stability in the presence of rotator cuff tears [15,16], and joint contact forces during alternative tasks such as weight relief lifts [e.g., 17,18]. These studies highlight the usefulness of simulations to investigate a number of unmeasurable quantities, such as muscle and joint contact forces, that may lead to shoulder pain and injury.

Recent studies have used modeling and simulation to investigate the upper extremity demands associated with propulsion technique [19,20]. One study demonstrated that each hand pattern has unique muscle power and stress requirements, with the SC and DL patterns requiring the least overall muscle demand [19]. Another study found that shoulder joint loading was decreased when participants used a larger contact angle and decreased cadence [20]. Although these propulsion characteristics are related to hand patterns, joint contact loading has not been examined across different hand patterns to provide insight into whether specific patterns might influence the shoulder's susceptibility to injury.

Shoulder muscle weakness is correlated with shoulder pain [21], and programs aimed at strengthening the shoulder adductors [22–24] and external rotators [24–26] are recommended for MWCU in order to decrease the risk of shoulder pain and impingement. However, how shoulder joint loading changes when specific muscle groups are weakened is still unknown. These changes are likely to vary between hand patterns [e.g., 19] as each hand pattern has unique muscle force demands. For example, SL and ARC tend to require more anterior and middle deltoid power [19] and modeling has shown that the anterior and middle deltoids and rotator cuff muscles tend to compensate for one another when weakened individually [27]. When combined with additional muscle weaknesses that require anterior and middle deltoid compensation, the SL and ARC patterns could further destabilize the glenohumeral joint and put the shoulder at risk of impingement [e.g., 15]. Therefore, evaluating how specific muscle group weakness affects shoulder joint loading across different hand patterns would provide further insight into factors contributing to the development of shoulder pain and injuries.

The purpose of this study was to identify how shoulder joint contact forces vary across recovery hand patterns to gain insight into shoulder pain and injury mechanisms. A secondary purpose was to determine how joint loading patterns change when the primary shoulder muscle groups (abductors, adductors, flexors, extensors, internal rotators, and external rotators) are weakened, and how the hand pattern used influences changes in shoulder joint loading due to muscle weakness. We expected that (1) hand patterns with higher anterior and middle deltoid forces, which elevate the humeral head (e.g., SL and ARC), will be accompanied by higher shoulder joint contact forces, and (2) weakening muscle groups with a majority of humeral head depressors (e.g., shoulder adductors, extensors, internal and external rotators) will cause increases in shoulder joint contact loading.

2 Methods

2.1 Experimental Data. Simulations were based on previously collected kinematic and kinetic data [23]. These data were collected at Rancho Los Amigos National Rehabilitation Center from MWCU with complete paraplegia and free from shoulder pain. Participants propelled their own wheelchair on a stationary ergometer during a 40-second trial at their self-selected speed, with data collected during the final 10 s during steady-state propulsion. Kinematic data were collected from the trunk, right-side upper extremity, and wheel using a 4-scanner CODA motion analysis system (Charnwood Dynamics Ltd., Leicestershire, UK) and 15 markers placed on body segment landmarks and the right wheel [28]. Three-dimensional kinetic data were collected from the right handrim using an instrumented wheel (SmartWheel; Out-Front, Pasco, WA). Kinematic and kinetic data were filtered in Visual3D (C-Motion, Inc., Germantown, MD) using low-pass, fourth-order, zero-lag Butterworth filters with cutoff frequencies of 6 and 10 Hz, respectively. A 5 N threshold for the resultant handrim force was used to identify the push and recovery phases of the propulsion cycle.

To determine each participant's hand pattern, the third metacarpophalangeal joint center (MCP3) was located using a previously described method [29] and the MCP3 trajectory was projected onto the handrim plane using custom Matlab (Mathworks, Natick, MA) code. Representative trajectories were created by averaging across cycles for each participant. Two quantitative parameters based on the hand's distance above the handrim and total distance from the handrim were calculated for each participant and used to classify which hand pattern was used by the individual [for details, see 30]. After classification, representative participants for each hand pattern were selected to minimize confounding factors that might influence the simulation results. Specifically, five individuals from each hand pattern group were selected based on level of spinal cord injury (T8-L5) and who produced the smallest root-mean-square differences in age, time from injury, height, mass, and propulsion speed from the group average (Table 1). Average data from these five individuals in each group were used to create group-averaged MCP3 trajectory, trunk, shoulder, elbow, and forearm angles and handrim force profiles for each hand pattern group. Then, a representative participant for each group was chosen whose average data best emulated the group-averaged data, and a representative cycle from that participant was selected using a functional median depth method with hand trajectory, handrim forces and joint angles as the criteria [31]. These representative propulsion cycles were then used to generate simulations for each hand pattern.

2.2 Musculoskeletal Model. An upper extremity musculoskeletal model developed by Saul et al. [32] and modified by McFarland et al. [33] was scaled to each representative participant using the experimental marker data and participant mass. The model consisted of trunk, right side upper arm, forearm, and hand segments, with a total of 13 degrees-of-freedom. Trunk lean over the whole propulsion cycle was prescribed based on the experimental kinematic data, clavicle and scapula motions were prescribed as a function of shoulder elevation [34], and the wrist was locked in the anatomical position. Thus, five degrees-of-freedom were independent: forearm pronation/supination, elbow flexion/extension, and shoulder plane-of-elevation, elevation angle and internal/external rotation angle [35].

Table 1 Hand pattern groups from which the representative propulsion cycles were chosen. Individuals were chosen such that differences between groups in age, time from injury, level of injury, height, mass and propulsion speed were minimized. All values are mean ± standard deviation.

Hand pattern group	Participant	Age (years)	Time from injury (years)	Level of injury	Height (m)	Mass (kg)	Propulsion speed (m/s)
Semicircular	1	32.9	14.6	T12	1.70	87.9	0.67
	2	34.6	1.9	T10	1.75	73.9	1.02
	3	22.8	2.1	T9	1.68	60.2	1.03
	4	**36.0**	**19.5**	**T10**	**1.73**	**74.4**	**0.73**
	5	32.8	13.1	T12	1.65	55.9	1.13
		31.8 ± 5.2	10.2 ± 7.9		1.70 ± 0.04	70.5 ± 12.7	0.92 ± 0.20
Arcing	6	22.1	3.5	T12	1.75	71.6	0.83
	7	**29.3**	**2.2**	**T12**	**1.65**	**85.5**	**0.90**
	8	41.5	10.0	T10	1.68	85.9	1.31
	9	40.1	4.8	T12	1.78	76.2	1.26
	10	25.3	8.0	T10	1.68	60.2	1.20
		31.6 ± 8.7	5.7 ± 3.2		1.71 ± 0.05	75.9 ± 10.7	1.10 ± 0.22
Single-loop	**11**	**42.2**	**1.8**	**T11**	**1.68**	**71.4**	**1.10**
	12	33.7	16.3	T12	1.73	68.1	1.34
	13	38.7	5.0	T12	1.63	65.5	1.07
	14	32.9	2.0	T10	1.70	83.1	0.90
	15	35.0	2.0	T12	1.70	87.6	1.02
		36.5 ± 3.9	5.4 ± 6.2		1.69 ± 0.03	75.1 ± 9.7	1.09 ± 0.16
Double-loop	16	36.6	2.9	T11	1.65	71.2	1.28
	17	**32.6**	**10.0**	**T9**	**1.68**	**65.9**	**0.90**
	18	25.5	4.8	T9	1.70	75.0	0.78
	19	39.3	13.3	T12	1.70	75.8	0.66
	20	31.7	2.3	L1	1.78	77.0	1.04
		33.1 ± 5.3	6.7 ± 4.8		1.70 ± 0.04	73.0 ± 4.5	0.93 ± 0.24
All		33.3 ± 5.9	7.0 ± 5.7		1.70 ± 0.04	73.6 ± 9.3	1.01 ± 0.21

The representative participant chosen from each group (based on hand trajectory, handrim forces and joint angles) is underlined.

Table 2 Upper extremity muscles included in the model

Muscle	Abbreviation	Origin	Insertion	Baseline maximum isometric force (N)
Deltoid				
Anterior	DELT1	Clavicle	Humerus	1218.9
Middle	DELT2	Scapula	Humerus	1103.5
Posterior	DELT3	Scapula	Humerus	201.6
Supraspinatus	SUPSP	Scapula	Humerus	499.2
Infraspinatus	INFSP	Scapula	Humerus	1075.8
Subscapularis	SUBSC	Scapula	Humerus	1306.9
Teres minor	TMIN	Scapula	Humerus	269.5
Teres major	TMAJ	Scapula	Humerus	144.0
Pectoralis major				
Clavicular	PECM1	Clavicle	Humerus	444.3
Sternal	PECM2	Throax	Humerus	658.3
Ribs	PECM3	Thorax	Humerus	498.1
Latissimus dorsi				
Thoracic	LAT1	Thorax	Humerus	290.5
Lumbar	LAT2	Throax	Humerus	317.5
Iliac	LAT3	Throax	Humerus	189.0
Coracobrachialis	CORB	Scapula	Humerus	208.2
Triceps				
Long	TRIlong	Scapula	Ulna	771.8
Lateral	TRIlat	Humerus	Ulna	717.5
Medial	TRImed	Humerus	Ulna	717.5
Anconeus	ANC	Humerus	Ulna	283.2
Supinator	SUP	Ulna	Radius	379.6
Biceps				
Long	BIClong	Scapula	Radius	525.1
Short	BICshort	Scapula	Radius	316.8
Brachialis	BRA	Humerus	Ulna	1177.4
Brachioradialis	BRD	Humerus	Radius	276.0
Pronator teres	PT	Humerus	Radius	557.2
Pronator quadratus	PQ	Ulna	Radius	284.7

Table 3 Upper extremity muscle groups that were weakened in each simulation. Muscles represent the prime power generators in each group.

Weakened simulation	Muscle	Abbreviation
Flexors		
	Anterior deltoid	DELT1
	Pectoralis major (clavicular)	PECM1
Extensors		
	Posterior deltoid	DELT3
	Teres major	TMAJ
	Latissimus dorsi	LAT1-3
Abductors		
	Middle deltoid	DELT2
	Supraspinatus	SUPSP
Adductors		
	Teres major	TMAJ
	Pectoralis major	PECM1-3
	Latissimus dorsi	LAT1-3
Internal rotators		
	Anterior deltoid	DELT1
	Subscapularis	SUBSC
	Teres major	TMAJ
	Pectoralis major	PECM1-3
	Latissimus dorsi	LAT1-3
External rotators		
	Posterior deltoid	DELT3
	Infraspinatus	INFSP
	Teres minor	TMIN

The model included 26 Hill-type musculotendon actuators [36] representing the primary muscles that cross the shoulder and elbow joints (Table 2). Previous work has found that shoulder moments are much higher than elbow and wrist joint moments [e.g., 37], and that the hand and forearm segments are used primarily for transferring power to the handrim, rather than generating power [e.g., 38]. Therefore, we chose to remove wrist and hand muscles (with the exception of wrist muscles contributing to forearm pronation/supination) in order to improve computational efficiency.

2.3 Simulation and Optimization Framework. Simulations were generated using OpenSim 4.0 [39]. First, individual joint angles were calculated using an inverse kinematics algorithm in order to minimize the error between experimental and model markers [39]. The resulting kinematics and experimental handrim forces (applied directly to the hand during the push phase, Fig. 7 in the Appendix) were used for tracking during simulations. A computed muscle control algorithm was used to determine the muscle excitations that reproduced the experimental kinematics while minimizing muscle activations squared [40,41]. The resulting muscle excitations were monitored to confirm that they were consistent with EMG timings reported in the literature [42–44] (Figs. 8–11 in the Appendix).

Baseline simulations of each hand pattern were generated using the baseline isometric muscle force values (Table 2). In the weakened simulations, muscles within each primary muscle group of interest (shoulder flexors, extensors, abductors, adductors, internal rotators and external rotators) were weakened by decreasing their peak isometric muscle force by 30% relative to the baseline model (Table 3). A reduction of 30% was chosen in order to provide a meaningful difference while still remaining within ranges of shoulder strength for MWCU [e.g., 45]. Excitations of the weakened muscles were constrained so that they could not exceed their baseline simulation values in order to ensure the muscles did not produce increased force through higher excitation levels.

2.4 Analysis. Seven simulations were analyzed for each of the four representative hand patterns (representing baseline strength and the six weakened conditions) for a total of 28 simulations. Glenohumeral joint contact forces (GJCF) for each simulation were determined using OpenSim's JointReaction analysis. The GJCF originates at the humeral head joint center and acts on the glenoid, and was transformed into the scapula's reference frame using custom Matlab code. The peak and impulse of the three independent components of the GJCF (i.e., anterior-posterior (shear), superior-inferior (shear) and medial (compressive)) were compared between each condition and across hand patterns. We chose to evaluate all three components of the GJCF separately in order to observe the shoulder's susceptibility to injury in each direction, since we were unable to enforce a stability constraint within the computed muscle control framework. Peak and impulse measures were selected because it is unclear whether a higher but less frequent force (peak) or moderate-to-high sustained forces over time (impulse) are more likely to result in shoulder pain or injuries. The peak forces and impulses were also compared in the push and recovery phases separately to determine their contributions during the full propulsion cycle. GJCF impulses were calculated by taking the time integral of the corresponding force during the push and recovery phases and over the full cycle.

3 Results

3.1 Tracking Kinematics. In the baseline simulations, the resulting kinematics closely replicated the joint angles from inverse kinematics for each participant, staying within one standard deviation (SD) of the experimental values. For the weakened simulations, kinematics for all joint angles remained within one SD of their experimental values, except for the DL pattern simulation with weakened internal rotators (Table 6 in the Appendix). In this simulation, the shoulder plane-of-elevation, elevation angle and rotation angle deviated outside one SD of the experimental values. (Figs. 12–15 in the Appendix). In addition, for all simulations, the resultant shoulder and elbow joint moments compared well with the corresponding moments determined using Visual3D (e.g., Fig. 16 in the Appendix).

3.2 Comparison Between Baseline Hand Patterns. Hand patterns with higher anterior and middle deltoid forces, which elevate the humeral head, were generally accompanied by higher GJCFs. The SL and DL patterns had the highest average anterior deltoid forces (74.3 N and 71.7 N, respectively) and had the highest superior GJCF impulses, while the SL and ARC patterns resulted in the highest average middle deltoid forces (168.3 N and 158.4 N, respectively) and the highest anterior GJCF impulses. The SC pattern had the lowest average anterior and middle deltoid forces (58.0 N and 138.7 N, respectively) and resulted in the lowest anterior and posterior and second-lowest superior GJCF impulses.

The SL and DL patterns had the highest and second-highest peak anterior GJCFs (Table 4), and the SL and ARC patterns had the highest and second-highest anterior GJCF impulses (Table 5), respectively. The SL and DL patterns had the highest posterior GJCF peaks and impulses (Figs. 2(*a*) and 2(*b*)).

The DL and ARC patterns had the highest and second-highest peak superior GJCFs, respectively (Fig. 2(*c*)). The DL and SL patterns had the highest and second-highest superior GJCF impulses, respectively (Fig. 2(*d*)).

The SL and ARC patterns had the highest and second-highest peak medial (i.e., compressive) GJCFs, respectively (Fig. 2(*e*)). The DL and SL patterns had the highest and second-highest medial GJCF impulses, respectively (Fig. 2(*f*)).

3.3 Comparison Between Weakness Conditions

3.3.1 Anterior-Posterior Glenohumeral Joint Contact Forces. Weakening the external rotators produced either the highest or second-highest anterior GJCF peak (Figs. 3(*a*)–6(*a*)) in the ARC, DL and SL hand patterns and the highest or second-highest anterior GJCF impulse in all patterns (Figs. 3(*b*)–6(*b*)). Weakening the extensors produced the second-highest peak anterior GJCF in the SC and DL patterns, and the second-highest anterior GJCF impulses in the ARC, DL and SL patterns. Weakening the adductors resulted in the highest anterior GJCF peak in the SC, ARC and SL patterns.

Table 4 Peak anterior-posterior, superior-inferior and medial glenohumeral joint contact forces (GJCFs) for all simulations during push and recovery

	Anterior (+)/Posterior (−) GJCF (N)				Superior (+)/Inferior (−) GJCF (N)				Medial (−) GJCF (N)	
	Positive peak		Negative peak		Positive peak		Negative peak		Negative peak	
	Push	Recovery	Push	Recovery	Push	Recovery	Push	Recovery	Push	Recovery
SC										
Baseline	103.90	47.34	−134.95	−182.68	166.35	281.39	−1.22	—	−280.33	−411.88
Adductors	153.38	37.32	−135.96	−171.86	168.75	245.72	−3.57	—	−268.05	−404.84
Abductors	106.81	—	−223.93	−299.92	94.99	122.47	−32.12	−28.31	−316.65	−450.67
External rotators	109.20	66.80	−120.28	−151.39	213.09	337.52	—	—	−269.88	−426.55
Internal rotators	55.16	51.84	−531.36	−234.21	213.60	269.93	—	—	−239.22	−324.46
Extensors	110.00	52.78	−129.71	−173.79	175.68	286.42	−13.99	—	−271.66	−468.10
Flexors	37.87	32.92	−136.46	−176.69	157.51	254.93	−11.04	—	−299.52	−390.37
ARC										
Baseline	126.28	62.43	−152.79	−241.90	170.02	289.91	—	—	−258.42	−414.94
Adductors	162.57	49.87	−134.54	−221.08	168.68	269.90	−9.96	—	−225.79	−375.64
Abductors	115.30	—	−246.01	−306.31	99.52	144.23	−34.73	−93.77	−329.30	−514.90
External rotators	149.99	100.87	−130.84	−184.84	254.63	353.54	—	—	−255.27	−428.60
Internal rotators	41.77	61.60	−518.97	−383.85	224.45	279.95	—	—	−222.11	−334.04
Extensors	130.45	73.60	−137.95	−236.92	172.49	302.32	−7.31	—	−253.48	−426.26
Flexors	45.10	49.21	−154.72	−229.11	162.86	264.92	—	—	−340.13	−372.27
SL										
Baseline	176.21	115.27	−210.58	−356.34	225.71	279.50	—	—	−324.46	−452.72
Adductors	238.21	98.45	−196.38	−342.64	219.92	272.67	—	—	−334.37	−423.50
Abductors	164.01	—	−327.22	−443.46	138.88	148.89	—	−120.18	−397.05	−743.55
External rotators	198.06	136.05	−173.47	−298.78	331.49	419.09	—	—	−330.00	−421.73
Internal rotators	90.19	95.75	−196.62	−334.62	176.41	386.82	—	—	−253.97	−435.72
Extensors	184.91	129.71	−204.12	−362.71	225.60	301.03	—	—	−316.58	−475.24
Flexors	79.62	94.07	−226.86	−347.04	223.73	262.81	—	—	−392.41	−432.07
DL										
Baseline	129.69	39.72	−223.26	−318.17	210.61	331.34	—	—	−314.96	−367.07
Adductors	130.74	31.27	−205.48	−312.04	193.23	310.86	—	—	−292.21	−352.86
Abductors	93.63	-	−306.22	−372.27	162.74	172.75	—	—	−377.67	−451.96
External Rotators	136.31	69.66	−181.59	−281.27	394.76	460.10	—	—	−337.53	−361.34
Internal Rotators	34.52	31.26	−289.58	−369.09	435.01	462.06	—	—	−396.47	−530.46
Extensors	131.80	53.23	−227.06	−333.48	180.33	346.55	—	—	−323.11	−392.91
Flexors	49.96	31.12	−206.75	−317.15	220.52	309.28	—	—	−343.43	−386.72

Table 5 Anterior-posterior, superior-inferior and medial glenohumeral joint contact force (GJCF) impulses for all simulations during push, recovery, and the full cycle

	Anterior (+)/Posterior (−) GJCF impulse (Ns)						Superior (+)/Inferior (−) GJCF impulse (Ns)						Medial (−) GJCF impulse (Ns)		
	Positive impulse			Negative impulse			Positive impulse			Negative impulse			Negative impulse		
	Push	Recovery	Full cycle	Push	Recovery	Full cycle	Push	Recovery	Full cycle	Push	Recovery	Full cycle	Push	Recovery	Full cycle
SC															
Baseline	18.88	3.91	22.79	−19.25	−75.50	−94.75	40.93	144.27	185.20	−0.02	—	−0.02	−148.71	−233.61	−382.32
Adductors	32.83	2.39	35.22	−19.44	−74.44	−93.88	55.74	127.32	183.07	−0.09	—	−0.09	−138.77	−221.94	−360.71
Abductors	18.71	—	18.71	−29.26	−150.68	−179.94	25.68	39.22	64.90	−2.75	−2.20	−4.95	−151.91	−297.36	−449.27
External rotators	24.11	6.73	30.84	−14.58	−54.25	−68.84	52.66	180.66	233.32	—	—	—	−145.27	−230.38	−375.66
Internal rotators	6.60	3.67	10.28	−70.18	−74.34	−144.52	64.99	148.34	213.33	—	—	—	−122.87	−183.53	−306.40
Extensors	21.15	4.13	25.28	−16.94	−73.29	−90.24	40.72	138.79	179.52	−0.36	—	−0.36	−145.26	−253.97	−399.23
Flexors	3.85	1.88	5.73	−27.03	−75.73	−102.76	27.75	131.18	158.94	−0.35	—	−0.35	−156.63	−220.92	−377.55
ARC															
Baseline	25.58	13.94	39.52	−9.89	−85.36	−95.24	40.24	135.77	176.01	—	—	—	−111.99	−271.46	−383.45
Adductors	32.08	8.47	40.55	−10.15	−78.31	−88.46	39.38	120.62	160.00	−0.08	—	−0.08	−101.22	−250.92	−352.14
Abductors	17.06	—	17.06	−18.26	−170.31	−188.56	23.47	35.39	58.86	−1.60	−18.55	−20.15	−120.79	−345.57	−466.36
External rotators	32.86	24.39	57.25	−8.55	−60.17	−68.72	46.35	198.05	244.40	—	—	—	−107.14	−260.80	−367.94
Internal rotators	6.03	6.46	12.49	−33.48	−82.02	−115.49	47.97	144.84	192.80	—	—	—	−90.56	−216.85	−307.41
Extensors	27.66	16.66	44.32	−9.88	−79.35	−89.24	36.37	131.97	168.34	−0.02	—	−0.02	−110.11	−284.68	−394.78
Flexors	4.15	7.65	11.80	−14.61	−84.34	−98.95	26.99	121.05	148.03	—	—	—	−130.70	−256.36	−387.06
SL															
Baseline	33.19	34.88	68.07	−16.52	−87.47	−103.99	69.80	151.44	221.24	—	—	—	−129.55	−255.07	−384.62
Adductors	41.18	27.44	68.62	−15.67	−83.61	−99.28	74.07	136.14	210.21	—	—	—	−123.82	−237.72	−361.54
Abductors	21.69	—	21.69	−34.59	−212.66	−247.25	43.62	39.52	83.14	—	−18.08	−18.08	−142.86	−391.28	−534.14
External rotators	37.94	45.12	83.06	−13.88	−69.15	−83.03	77.56	203.53	281.09	—	—	—	−126.03	−247.20	−373.23
Internal rotators	9.36	27.18	36.54	−39.03	−79.79	−118.81	46.60	147.02	193.61	—	—	—	−92.45	−210.66	−303.11

Table 5 (continued)

	Anterior (+)/Posterior (−) GJCF impulse (Ns)						Superior (+)/Inferior (−) GJCF impulse (Ns)						Medial (−) GJCF impulse (Ns)		
	Positive impulse			Negative impulse			Positive impulse			Negative impulse			Negative impulse		
	Push	Recovery	Full cycle	Push	Recovery	Full cycle	Push	Recovery	Full cycle	Push	Recovery	Full cycle	Push	Recovery	Full cycle
Extensors	34.81	41.33	76.14	−15.83	−86.22	−102.05	67.25	154.76	222.00	—	—	—	−125.36	−269.69	−395.05
Flexors	9.11	23.89	33.00	−19.81	−93.04	−112.85	54.71	133.93	188.64	—	—	—	−147.37	−253.58	−400.95
DL															
Baseline	32.12	5.36	37.48	−18.20	−154.48	−172.67	89.34	211.97	301.31	—	—	—	−133.36	−307.08	−440.44
Adductors	31.13	3.89	35.02	−18.18	−147.02	−165.20	85.31	193.68	278.99	—	—	—	−123.33	−287.93	−411.26
Abductors	17.53	—	17.53	−31.87	−263.97	−295.84	63.58	82.33	145.91	—	—	—	−144.33	−389.91	−534.24
External rotators	33.80	10.97	44.77	−15.46	−125.26	−140.72	92.68	291.36	384.03	—	—	—	−125.70	−297.46	−423.16
Internal rotators	2.20	2.36	4.56	−39.27	−145.67	−184.94	106.01	224.19	330.20	—	—	—	−124.53	−276.99	−401.52
Extensors	30.16	7.46	37.62	−18.04	−155.05	−173.08	77.92	206.53	284.45	—	—	—	−125.69	−323.73	−449.42
Flexors	11.42	3.10	14.52	−19.18	−150.16	−169.34	74.32	197.23	271.55	—	—	—	−156.65	−294.16	−450.81

In the posterior direction, weakening the abductors resulted in the highest or second-highest peak posterior GJCF and highest posterior GJCF impulse in all hand patterns, and weakening the internal rotators resulted in the highest or second-highest peak posterior GJCF in the SC, ARC and DL patterns. Similarly, the weakened internal rotators simulations produced the second-highest posterior GJCF impulse in all hand patterns.

3.3.2 Superior-Inferior Glenohumeral Joint Contact Forces. In all hand patterns, weakening the external rotators resulted in the highest superior GJCF peak (Figs. 3(*c*)–6(*c*)) and impulse (Figs. 3(*d*)–6(*d*)). In addition, weakening the internal rotators resulted in the second-highest peak superior GJCF in the DL and SL patterns, and the second-highest peak superior GJCF impulses in the SC, ARC and DL patterns. Weakening the abductors resulted in the highest peak inferior (most negative) GJCF and inferior GJCF impulse for the SC, ARC and SL patterns, and the lowest superior peak GJCF and superior GJCF impulse in the DL pattern.

3.3.3 Medial Glenohumeral Joint Contact Forces. The peak medial (most negative) GJCF occurred in the weakened abductors simulation in the ARC and SL hand patterns (Figs. 3(*e*)–6(*e*)). The

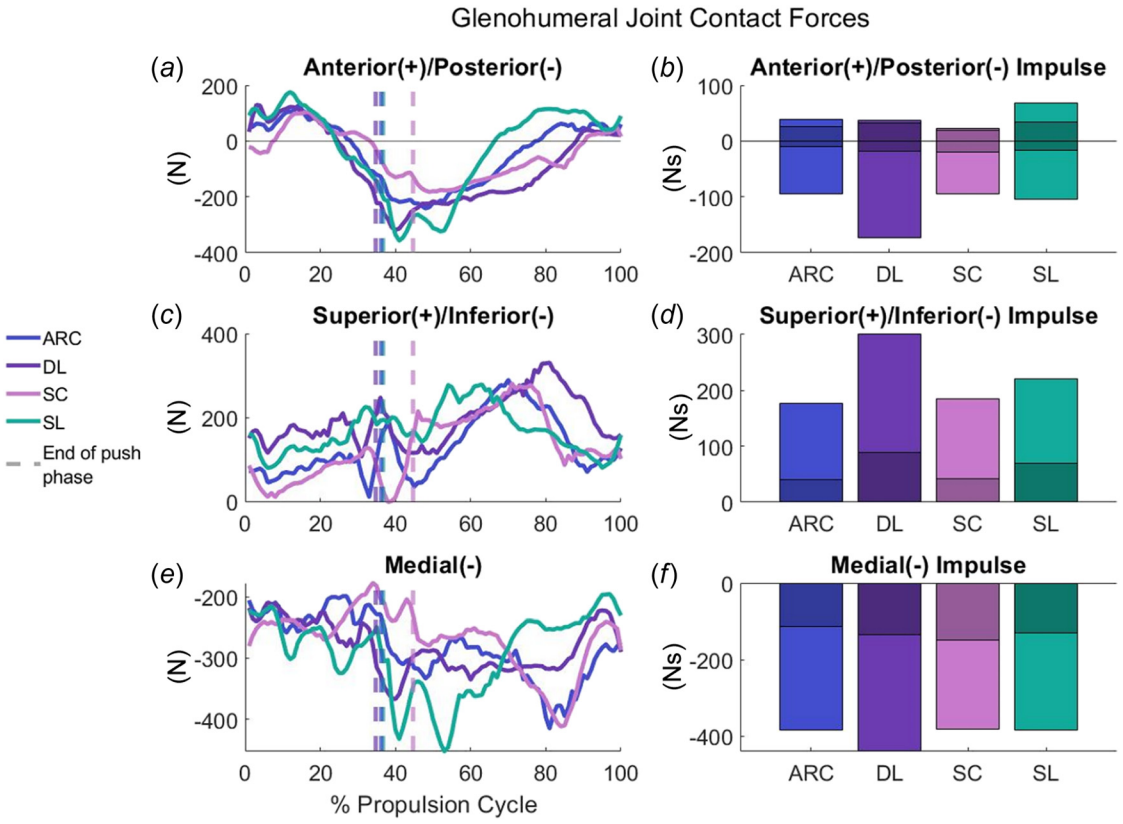

Fig. 2 Anterior-posterior (*a*–*b*), superior-inferior (*c*–*d*) and medial (*e*–*f*) glenohumeral joint contact forces (GJCFs) over the full cycle (*a*, *c*, *e*) and GJCF impulses (*b*, *d*, *f*) for the arcing (ARC), double-loop (DL), semicircular (SC) and single-loop (SL) baseline simulations. Darker shaded regions indicate contributions to the GJCF impulse during the push phase (*b*, *d*, *f*). Note: *y* axes are scaled to the data and not consistent between graphs.

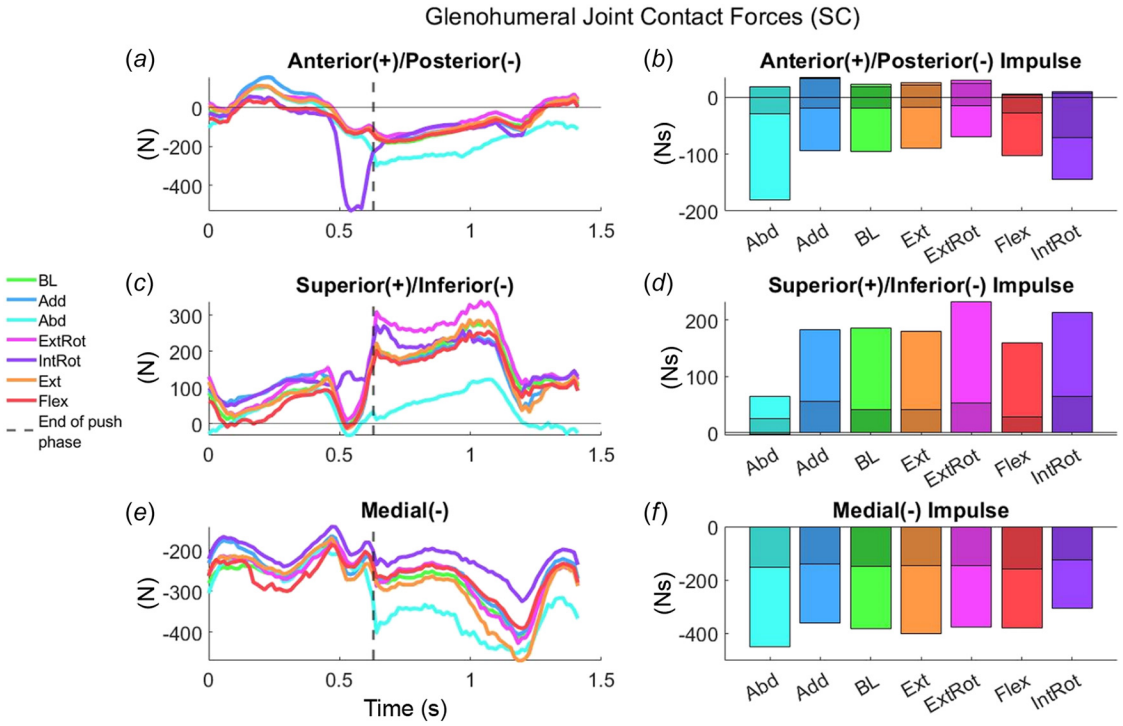

Fig. 3 Anterior-posterior (*a*–*b*), superior-inferior (*c*–*d*) and medial (*e*–*f*) glenohumeral joint contact forces (GJCFs) over the full cycle (*a*, *c*, *e*) and GJCF impulses (*b*, *d*, *f*) for all the semicircular (SC) pattern simulations. Shaded regions indicate contributions to the GJCF impulse during the push phase (*b*, *d*, *f*). Note: *y* axes are scaled to the data and not consistent between graphs.

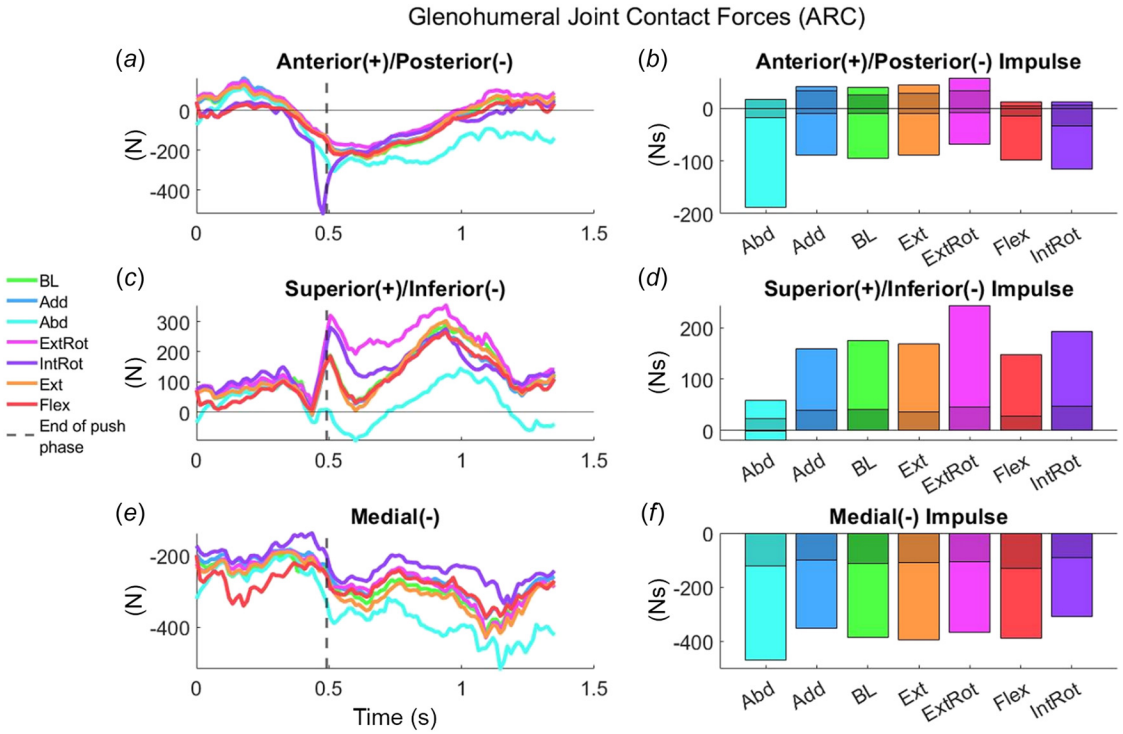

Fig. 4 Anterior-posterior (*a*–*b*), superior-inferior (*c*–*d*) and medial (*e*–*f*) glenohumeral joint contact forces (GJCFs) over the full cycle (*a*, *c*, *e*) and GJCF impulses (*b*, *d*, *f*) for all the arcing (ARC) pattern simulations. Shaded regions indicate contributions to the GJCF impulse during the push phase (*b*, *d*, *f*). Note: *y* axes are scaled to the data and not consistent between graphs.

peak medial GJCF occurred in the weakened internal rotators simulation for the DL pattern and in the weakened extensors simulation for the SC pattern. Weakening the abductors resulted in the highest medial GJCF impulse in all patterns (Figs. 3(*f*)–6(*f*)).

4 Discussion

This study compared GJCFs between four commonly used hand patterns and determined how those forces change when primary shoulder muscle groups are weakened. We expected that hand patterns with increased anterior and middle deltoid forces would correspond to higher GJCFs, which was partially supported. Patterns with higher anterior deltoid forces had higher superior GJCFs. However, the middle deltoid forces were very similar between patterns. We also expected that weakening the adductors, extensors, internal rotators and external rotators would result in increased GJCFs, which was also partially supported. In general, weakening the external rotators did increase anterior and superior shear forces while decreasing compressive forces, and weakening the internal rotators resulted in large peaks in the GJCFs with decreased compressive force impulses. However, weakening the adductors and extensors did not produce substantial changes in the GJCFs compared to the baseline conditions.

The magnitude of the GJCFs were in agreement with previous work [e.g., 17,46–48], where peak resultant force values ranged from 350 to 800 N, and peak resultant force values from the baseline simulations ranged from 450 to 600 N. In the present study, peak values occurred in the recovery phase, unlike other work that found peak GJCFs occur during the push phase [e.g., 48]. During the push-to-recovery phase transition, the inertial forces of the arm require the muscles to activate in order to slow down and reverse the direction of the arm [14]. Furthermore, the experimentally determined shoulder joint intersegmental forces, which include inertial forces and external forces but not compressive muscle forces [49], also peak in the early recovery phase (e.g., Fig. 17 in the Appendix). This confirms that inertial forces are quite high in this region, as external forces from the handrim are not present, and contributions from gravity to the intersegmental forces are typically low. Other work that found GJCFs peaked in the early recovery phase also found that this peak coincided with joint intersegmental forces [17]. Therefore, these inertial forces require high muscle forces in the early recovery phase to reverse the arm movement, which increases the GJCFs.

4.1 Tracking Kinematics. The DL pattern with weakened internal rotators was the only simulation that was not able to replicate the kinematics within one SD of the experimental values. In an effort to understand why, we ran an induced acceleration analysis posthoc to determine which muscles contribute to the acceleration of the shoulder angles. In the DL baseline simulation, the subscapularis was the highest contributor to the acceleration of shoulder plane-of-elevation during the recovery phase, which is not the case for the other hand patterns. Subscapularis is a primary internal rotator, and therefore weakened in this simulation. Consequently, the DL weakened internal rotators simulation kinematics are affected by subscapularis weakness more than the other patterns. In addition, subscapularis is also a primary contributor to both shoulder elevation and rotation angles for all hand patterns during the recovery phase. In fact, all shoulder muscles contribute to the acceleration of more than one shoulder angle [50]. Therefore, deviations due to muscle weakness in any one of these shoulder angles could make it more challenging for the other shoulder angles to track the experimental values, which is likely why the shoulder elevation and rotation angles also deviated outside of one SD of the experimental values in this simulation.

4.2 Comparison Between Baseline Hand Patterns. The SC and ARC patterns had the lowest anterior and posterior GJCFs, while the SL pattern had the highest anterior GJCFs. Generally,

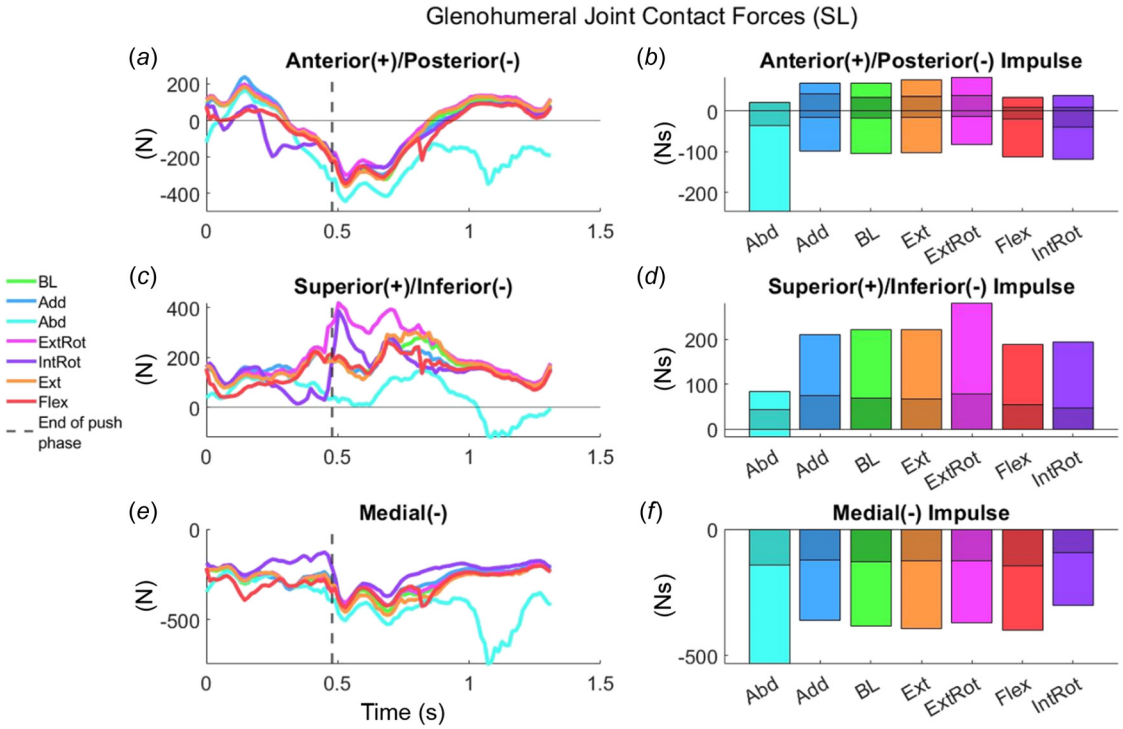

Fig. 5 Anterior-posterior (*a*–*b*), superior-inferior (*c*–*d*) and medial (*e*–*f*) glenohumeral joint contact forces (GJCFs) over the full cycle (*a*, *c*, *e*) and GJCF impulses (*b*, *d*, *f*) for all the single-loop (SL) pattern simulations. Shaded regions indicate contributions to the GJCF impulse during the push phase (*b*, *d*, *f*). Note: *y* axes are scaled to the data and not consistent between graphs.

increases in anterior GJCFs act to decrease shoulder joint stability [51]. However, either anteriorly- or posteriorly-directed forces are still shear in nature and should be minimized to reduce the potential for injury or dislocation. In fact, the anterior and posterior directions have a much lower threshold for dislocation than the superior-inferior direction [52]. Therefore, the SC pattern had the most favorable GJCFs than the other patterns in the anterior-posterior direction.

The DL and SL patterns had higher superior GJCF impulses than the SC and ARC patterns, and the DL pattern had the highest peak superior GJCF. Previous work found that anterior and middle deltoid forces were significant contributors to the superior GJCF [53]. Therefore, the increased superior GJCF in the DL and SL patterns may be attributed to the higher peak anterior deltoid force in these patterns compared to ARC and SC (Fig. 18 in the Appendix). Even though superior-inferior joint contact force is less susceptible to joint dislocation than in the anterior-posterior direction [52], increased superior forces at the shoulder are often associated with the potential for subacromial impingement [e.g., 54]. Therefore, the lower superior GJCF in the SC and ARC patterns suggests that using one of these patterns is less likely to contribute to pathologies such as shoulder impingement.

Unlike the anterior-posterior and superior-inferior directions, having increased medial force is preferred because the medial force keeps the humeral head compressed against the glenoid fossa, which allows the glenohumeral joint to withstand more shear force [52]. Because the glenohumeral joint used in this study is fixed and therefore inherently stable, decreased compressive force will not destabilize the joint, and increased compressive force will not further stabilize the joint. Therefore, increased compressive GJCF in these simulations does not necessarily indicate any increased or decreased risks for injury, but rather provides insight into which muscles should be strengthened to avoid overuse injury, as they will be needed not just for propulsion demands, but will have increased demands when needed to stabilize the glenohumeral joint [51]. We found that the DL pattern had the highest compressive force impulse, and the SL and ARC patterns had the highest and second-highest peak compressive force. These compressive force peaks may be due to the activity of the rotator cuff muscles. Previous work found that the lines of action of the rotator cuff muscles provide compressive force to the glenohumeral joint [55]. In the early recovery phase, the SC pattern had a much lower peak infraspinatus force than the other patterns, which may contribute to its lower compressive force (Fig. 18 in the Appendix). Similarly, other work found that the SC pattern had decreased muscle activity from the recovery phase muscles in the late push phase (i.e., less cocontraction during the transition) than self-selected patterns [6]. Therefore, rehabilitation programs for MWCU should seek to increase cocontraction during the push-to-recovery-phase transition, where more muscle activity is needed to help slow down and change direction of the arm [14], and strengthen the rotator cuff muscles, which provide power to the arm during both push (infraspinatus) and recovery (subscapularis) [14] and whose forces will increase when stability is required [56].

4.3 Comparison Between Weakness Conditions. In all hand patterns, weakening the internal rotators produced large peaks in the GJCFs in the transition region. The subscapularis is weakened in the weakened internal rotators simulation, and is active at the end of the push phase and early recovery phase to reposition the hand and accelerate it posterior [14]. Since the subscapularis cannot produce as much force in the weakened internal rotators condition, the simulation increased posterior deltoid and biceps activity to compensate, resulting in a large peak posterior deltoid and biceps long head force, and consequently large posterior (SC and ARC),

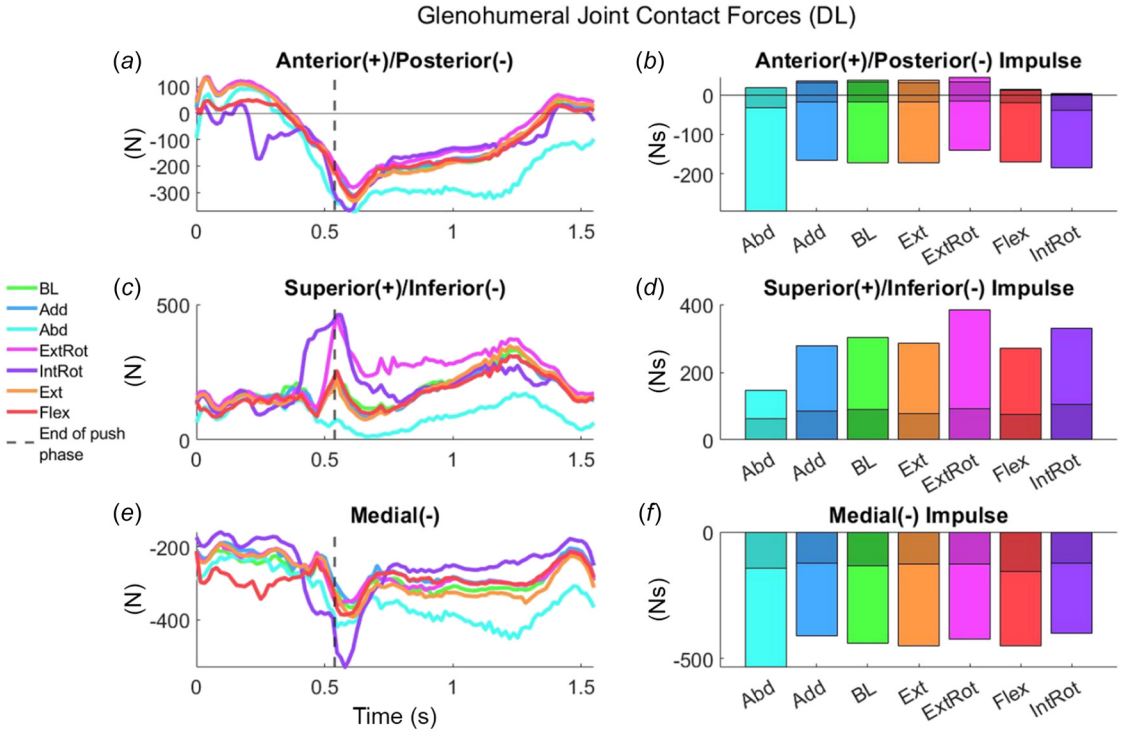

Fig. 6 Anterior-posterior (*a*–*b*), superior-inferior (*c*–*d*) and medial (*e*–*f*) glenohumeral joint contact forces (GJCFs) over the full cycle (*a*, *c*, *e*) and GJCF impulses (*b*, *d*, *f*) for all the double-loop (DL) pattern simulations. Shaded regions indicate contributions to the GJCF impulse during the push phase (*b*, *d*, *f*). Note: *y* axes are scaled to the data and not consistent between graphs.

superior (all patterns) and compressive (DL) GJCF peaks [53] (see excitations, Figs. 8–11 in the Appendix). The biceps long head pulls the humeral head downward to prevent upward migration [57], and other work that simulated rotator cuff tears found that biceps muscle force increased when supraspinatus, infraspinatus and subscapularis tears were present, resulting in more posterior and superior GJCFs [15]. Weakening the internal rotators also resulted in decreased compressive force impulses, despite the compressive force peak that occurs in the DL patterns. This decrease in compressive force impulse is likely due to decreases in infraspinatus and subscapularis forces (see excitations, Figs. 8–11 in the Appendix), which provide glenohumeral joint compression [52]. Therefore, having weakened internal rotators increases glenohumeral joint shear forces, likely putting MWCU at risk of shoulder injury, particularly during the transition region of the propulsion cycle, regardless of the hand pattern used.

Weakening the external rotators increased shear force in both the anterior and superior directions, and slightly decreased compressive GJCFs for all hand patterns. Increases in the superior direction were likely caused by increased force from the middle deltoid, a significant contributor to superior glenohumeral shear force [53] (see excitations, Figs. 8–11 in the Appendix). In addition, similar to the internal rotators, weakening the external rotators caused decreases in infraspinatus and subscapularis activity, likely causing the decreased compressive force. Therefore, weakened external rotators may make MWCU more susceptible to shoulder injuries like subacromial impingement, regardless of hand pattern used.

An interesting result was that weakening the adductors and extensors did not elicit large differences from the baseline simulations, contrary to our expectations. Although the adductors and extensors contain a majority of humeral head depressors, these muscle groups do not contain any rotator cuff muscles. Therefore, the changes in GJCFs occurring in the weakened internal and external rotators simulations combined with the lack of change in GJCFs in the weakened adductors and extensors simulations are likely attributed to sufficient compensation from the rotator cuff muscles. Therefore, strengthening the rotator cuff muscles, namely, the infraspinatus, supraspinatus, subscapularis and teres minor may be the most effective strategy for keeping shear GJCFs low and avoiding overuse muscle injuries, considering increases in rotator cuff muscle forces will be needed for maintaining stability [56].

Another interesting result was that for all hand patterns, weakening the abductors increased compressive forces and decreased anterior and superior shear forces, although posterior shear forces increased. Weakening the abductors weakened the middle deltoid, which produced an increase in posterior deltoid, infraspinatus and subscapularis activity to compensate, agreeing with previous work that found that weakening the middle and posterior deltoid increased subscapularis and infraspinatus muscle power [27]. Therefore, this decreased muscle force from the middle deltoid and subsequent increase from the posterior deltoid likely decreased the superior and anterior (and increased posterior) GJCFs, respectively. In addition, increases in infraspinatus and subscapularis activity likely increased the compressive forces. A previous study implementing a strengthening program that targeted the rotator cuff, specifically the infraspinatus and supraspinatus, found decreases in shoulder pain [26]. Therefore, the results of the present study further highlight the need for MWCU to strengthen the rotator cuff muscles in order to help reduce shear GJCFs that occur from the deltoids and put the shoulder at risk of shoulder pain and injury.

4.4 Limitations. A potential limitation of this study is that the simulations did not enforce shoulder stability. As the shoulder muscles produce force to propel the wheelchair, the shoulder musculature is also required to keep the humeral head within the glenoid to prevent shoulder impingement or dislocation [e.g., 51,53]. We were unable to add a stability constraint to the computed muscle control optimization framework, and therefore could not enforce the stability of the shoulder. Instead, we chose to address the shoulder's susceptibility to injury in each direction by comparing between hand patterns and with and without shoulder weakness. However, we believe that analyzing wheelchair propulsion with glenohumeral joint stability enforced is the next critical step for future work to aid in the prevention of shoulder injuries. Another limitation of this model is that we could not include humeral head translation or independent scapula motion. Future simulation work should seek to understand how GJCFs affect humeral head translation as well as the role of the scapula muscles during wheelchair propulsion. Another potential limitation is the assumption that muscle weakness would not change the resulting kinematics. We believe that keeping the kinematics constant allowed us to determine how muscle weakness alone affects the GJCFs without the confounding effect of changing kinematics. However, future work should use predictive simulations to analyze the relationship between changes in shoulder strength and the resulting kinematics. Finally, despite our efforts, there still exist small differences in a number of potential confounding demographic factors in our participants (Table 1). Because these factors were not equal for every individual, there is likely some natural variability in GJCFs for this population. Therefore, caution should be taken before recommending a specific hand pattern to all MWCU without considering patient-specific needs.

4.5 Summary. In conclusion, the SC pattern consistently had lower shear (anterior-posterior and superior-inferior) GJCFs compared to other patterns, and the DL and SL patterns had the highest shear GJCFs. These results suggest that using the SC pattern is less susceptible to shoulder injuries such as subacromial impingement than other patterns. However, MWCU should work to increase cocontraction during the push-to-recovery phase transition where joint stiffness is needed. In the presence of muscle weakness, weakening the internal rotators and external rotators resulted in the greatest increases in shear GJCFs and decreases in compressive GJCF, likely due to weakened rotator cuff muscles. Therefore, strengthening these muscle groups, especially the rotator cuff, is needed for decreasing the risk of shoulder injuries.

Appendix

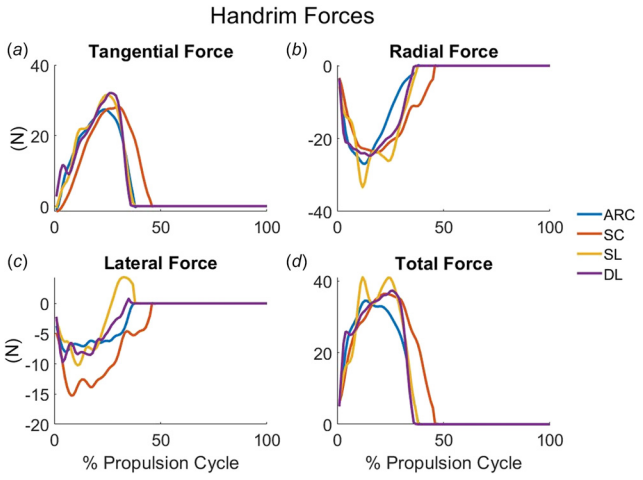

Fig. 7 The experimental handrim forces collected from the pushrim for the representative arcing (ARC), semicircular (SC), single-loop (SL) and double-loop (DL) simulations, which were applied to the hand segment during the simulations. Note: handrim force *x*-, *y*- and *z*-components were applied to the hand, but were transformed into their tangential (*a*), radial (*b*), and lateral (*c*) force components here.

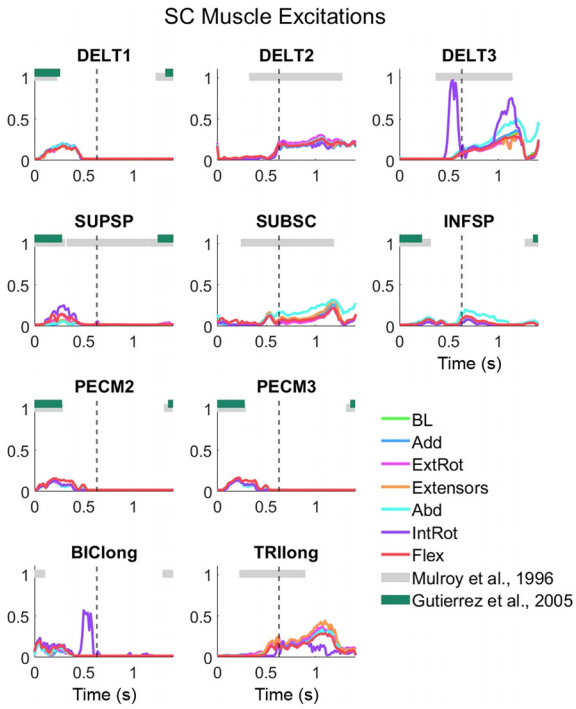

Fig. 8 Excitation timings for the anterior, middle and posterior deltoids (DELT1-3, respectively), supraspinatus (SUPSP), subscapularis (SUBSC), infraspinatus (INFSP), sternal pectoralis major (PECM2-3), biceps long head (BIClong) and triceps long head (TRIlong) in the semicircular (SC) baseline (BL) simulation and weakened simulations (Add, ExtRot, Extensors, Abd, IntRot, Flex). Shaded, horizontal bars represent EMG timings from the literature [43,44]. Dashed vertical line indicates the end of the push phase.

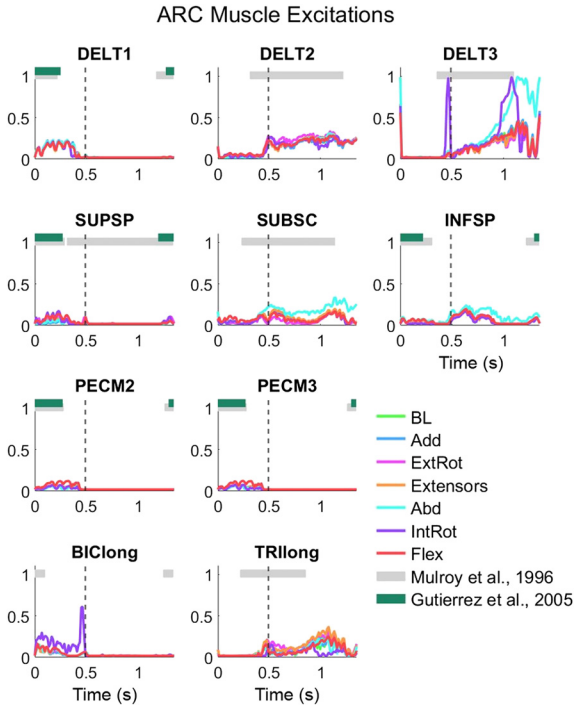

Fig. 9 Excitation timings for the anterior, middle and posterior deltoids (DELT1-3, respectively), supraspinatus (SUPSP), subscapularis (SUBSC), infraspinatus (INFSP), sternal pectoralis major (PECM2-3), biceps long head (BIClong) and triceps long head (TRIlong) in the arcing (ARC) baseline (BL) simulation and weakened simulations (Add, ExtRot, Extensors, Abd, IntRot, Flex). Shaded, horizontal bars represent EMG timings from the literature [43,44]. Dashed vertical line indicates the end of the push phase.

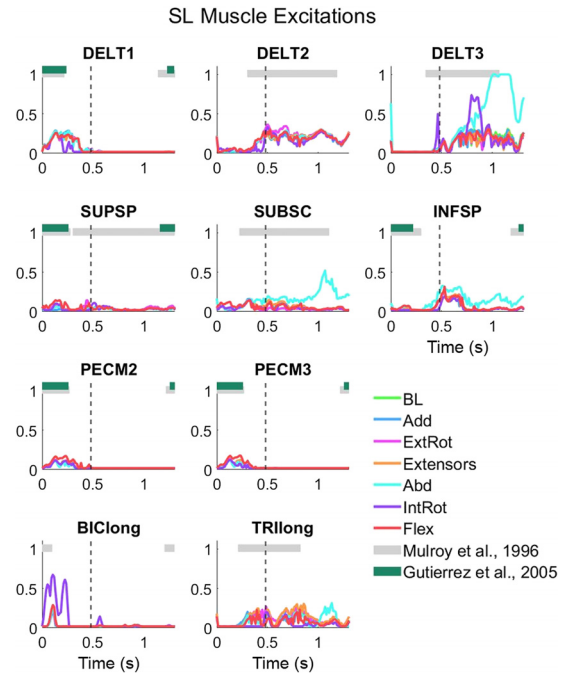

Fig. 10 Excitation timings for the anterior, middle and posterior deltoids (DELT1-3, respectively), supraspinatus (SUPSP), subscapularis (SUBSC), infraspinatus (INFSP), sternal pectoralis major (PECM2-3), biceps long head (BIClong) and triceps long head (TRIlong) in the single-loop (SL) baseline (BL) simulation and weakened simulations (Add, ExtRot, Extensors, Abd, IntRot, Flex). Shaded, horizontal bars represent EMG timings from the literature [43,44]. Dashed vertical line indicates the end of the push phase.

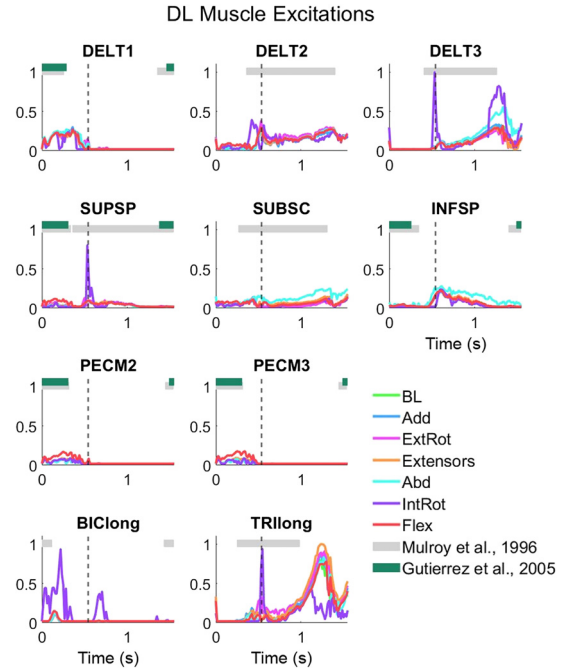

Fig. 11 Excitation timings for the anterior, middle and posterior deltoids (DELT1-3, respectively), supraspinatus (SUPSP), subscapularis (SUBSC), infraspinatus (INFSP), sternal pectoralis major (PECM2-3), biceps long head (BIClong) and triceps long head (TRIlong) in the double-loop (DL) baseline (BL) simulation and weakened simulations (Add, ExtRot, Extensors, Abd, IntRot, Flex). Shaded, horizontal bars represent EMG timings from the literature [43,44]. Dashed vertical line indicates the end of the push phase.

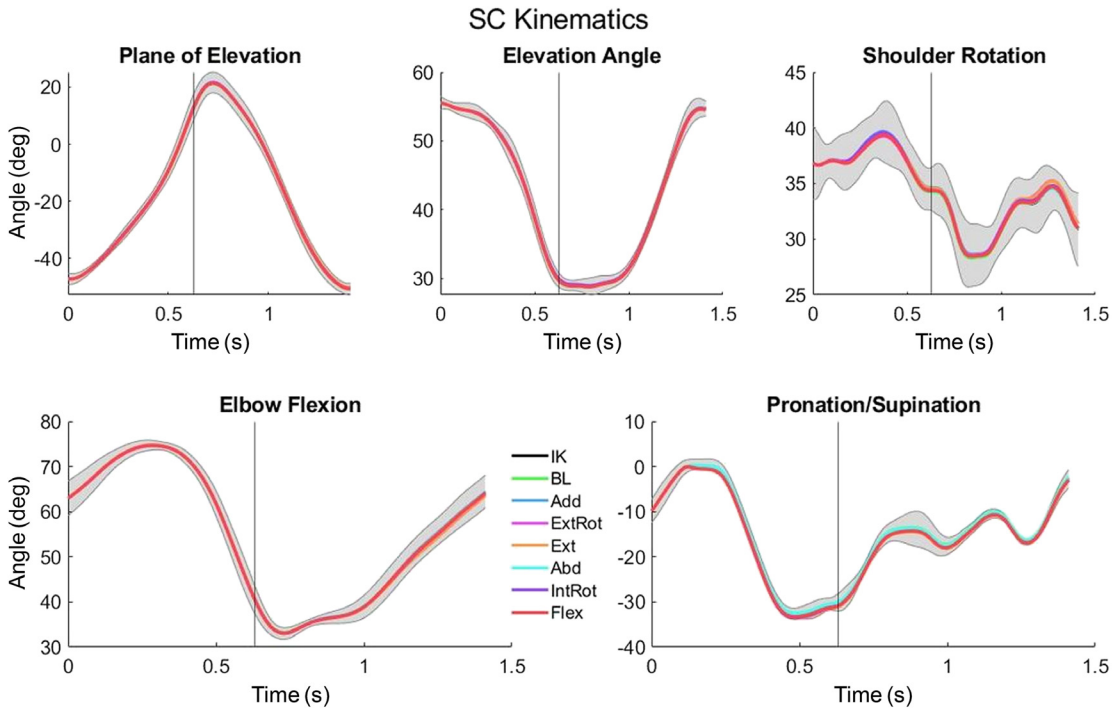

Fig. 12 Semicircular (SC) pattern kinematics for the baseline (BL) and weakened simulations. IK indicates the experimental kinematic results from the inverse kinematics algorithm, and shaded regions are ±1 standard deviation of the participant's experimental values. Vertical lines indicate the end of push phase.

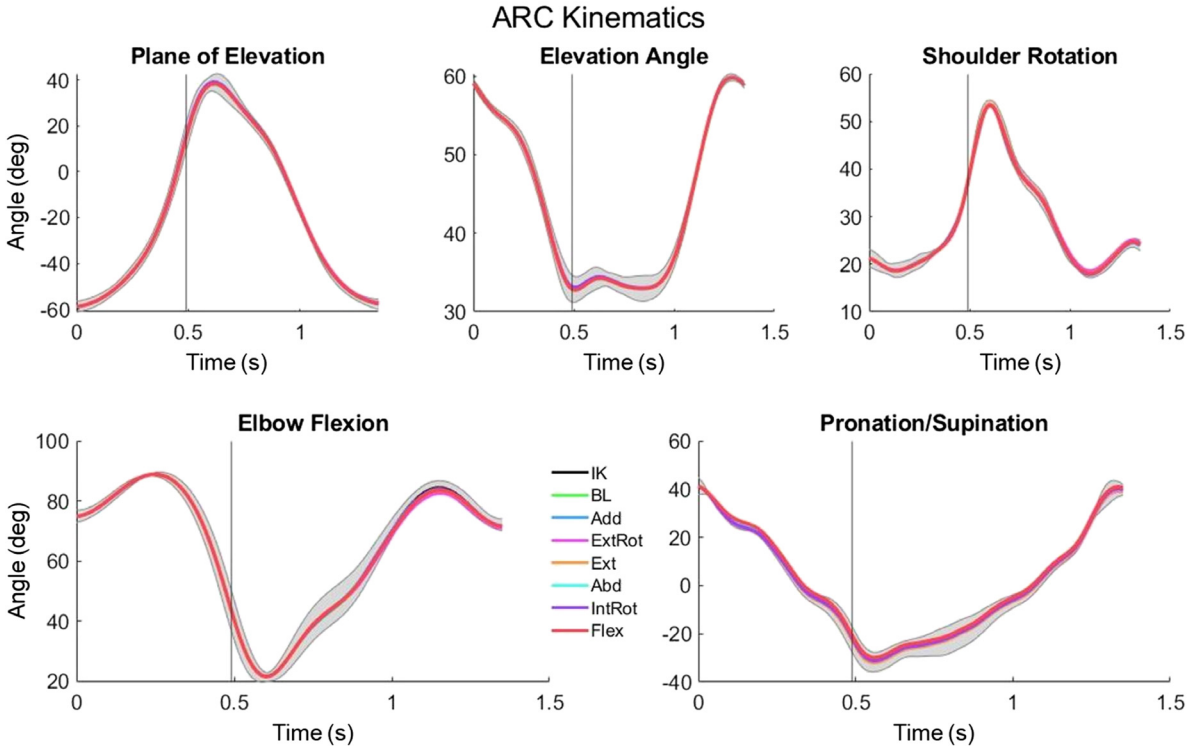

Fig. 13 Arcing (ARC) pattern kinematics for the baseline (BL) and weakened simulations. IK indicates the experimental kinematic results from the inverse kinematics algorithm, and shaded regions are ±1 standard deviation of the participant's experimental values. Vertical lines indicate the end of push phase.

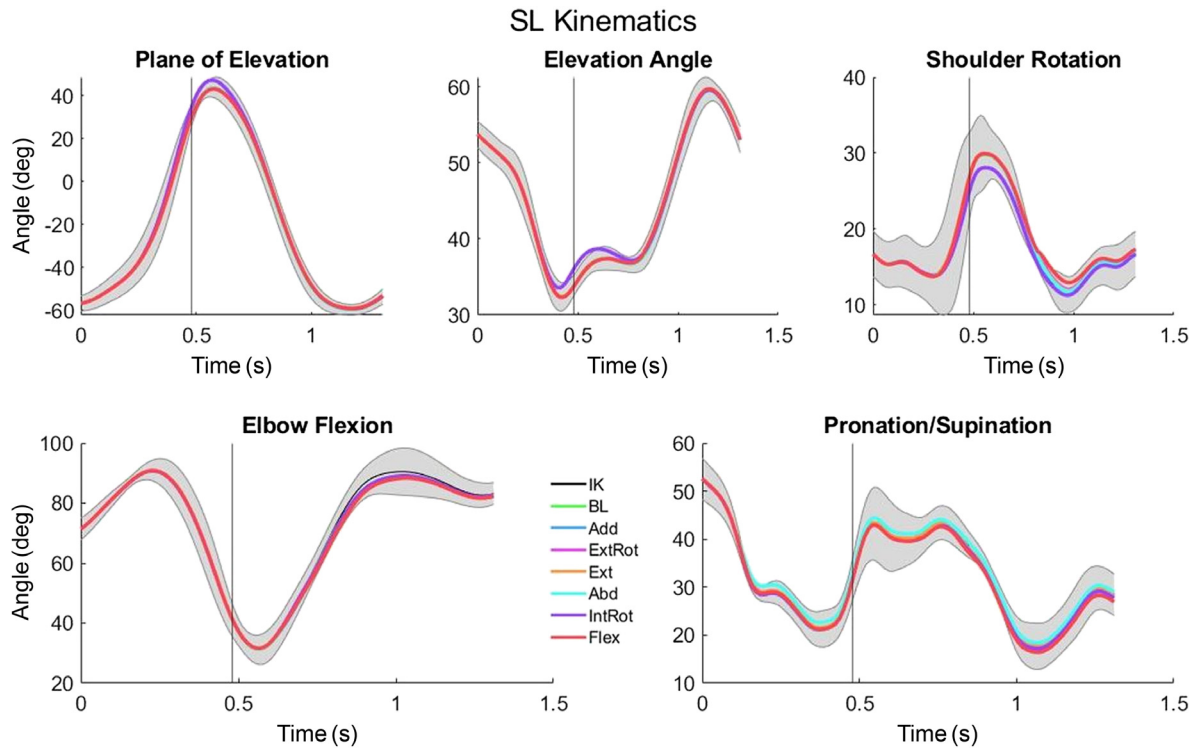

Fig. 14 Single-loop (SL) pattern kinematics for the baseline (BL) and weakened simulations. IK indicates the experimental kinematic results from the inverse kinematics algorithm, and shaded regions are ±1 standard deviation of the participant's experimental values. Vertical lines indicate the end of push phase.

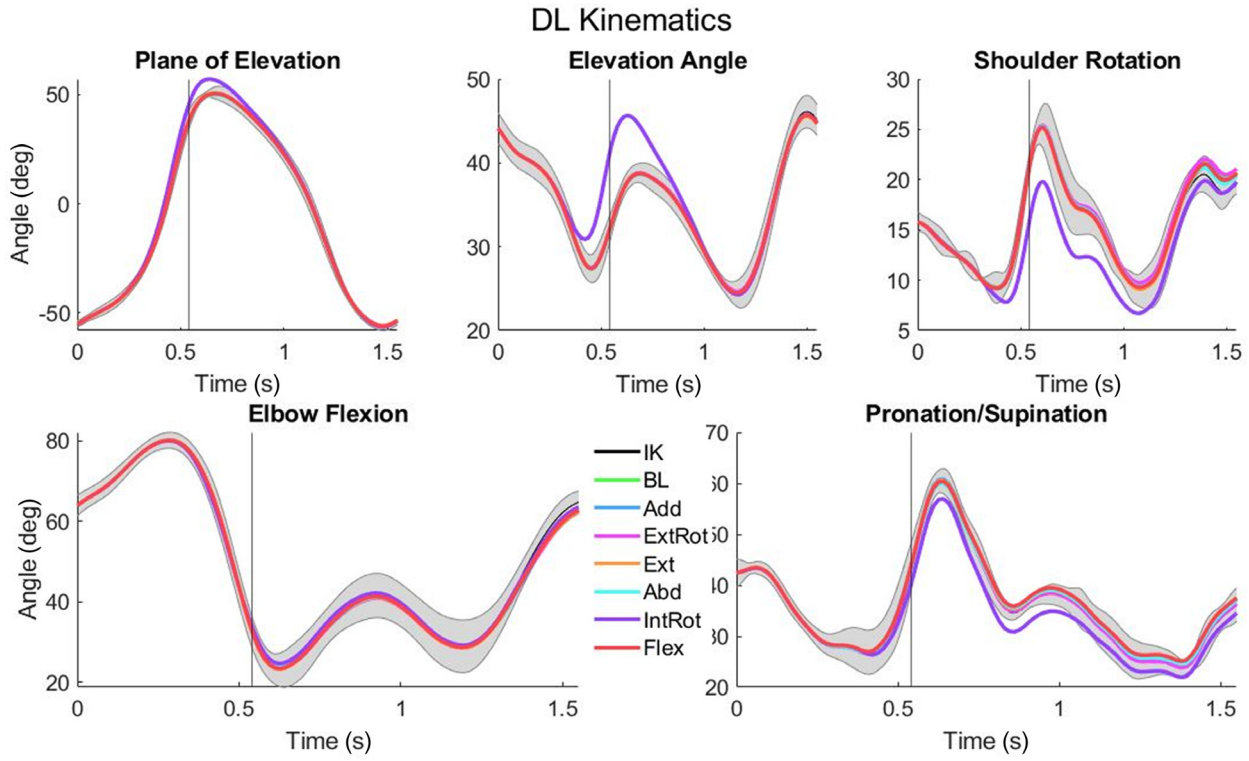

Fig. 15 Double-loop (DL) pattern kinematics for the baseline (BL) and weakened simulations. IK indicates the experimental kinematic results from the inverse kinematics algorithm, and shaded regions are ±1 standard deviation of the participant's experimental values. Vertical lines indicate the end of push phase.

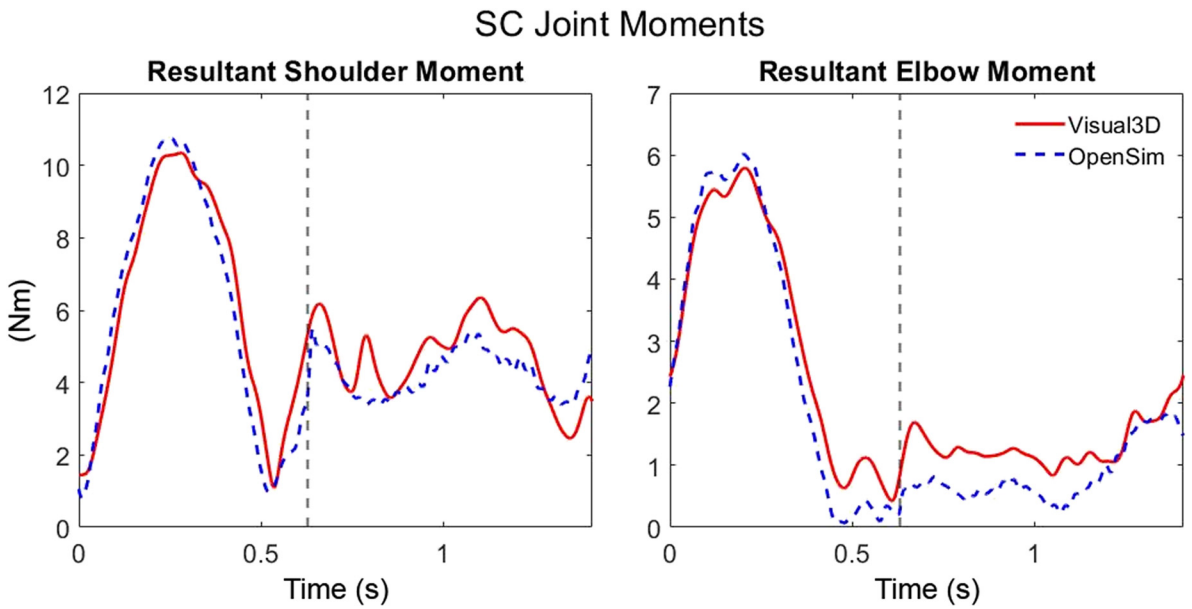

Fig. 16 Resultant shoulder and elbow moments determined in Visual3D (solid) and OpenSim (dashed) for the propulsion cycle chosen to represent the semicircular (SC) pattern. Dashed vertical lines indicate the end of the push phase.

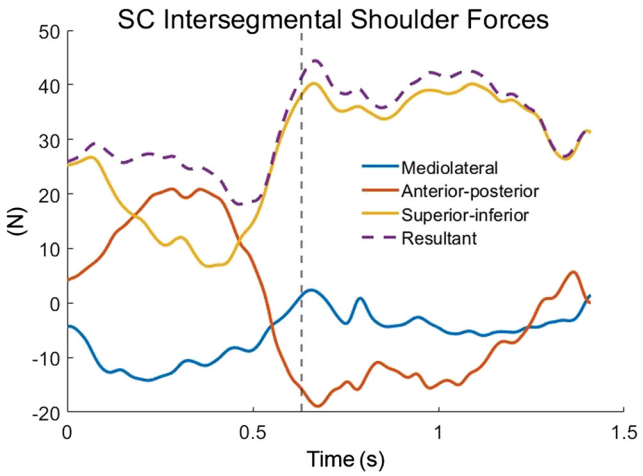

Fig. 17 Shoulder joint intersegmental forces determined using inverse dynamics for the semicircular (SC) pattern. Dashed vertical line indicates the end of the push phase.

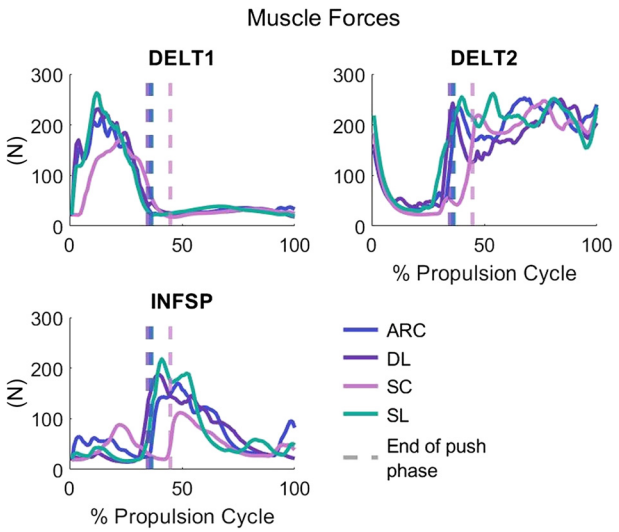

Fig. 18 Muscle forces during the propulsion cycle for the anterior deltoid (DELT1), middle deltoid (DELT2) and infraspinatus (INFSP) for the arcing (ARC), double-loop (DL), semicircular (SC), and single-loop (SL) baseline simulations

Table 6 Average kinematic RMS errors between each simulation and the inverse kinematics results. For comparison, 1 SD for that participant's experimental data is shown in parentheses in each baseline simulation row. Underlined values indicate average kinematic errors that exceed 1 SD. All values are in degrees.

	Plane-of-elevation	Elevation angle	Shoulder rotation	Elbow flexion	Pronation supination
SC					
Baseline	0.187 (2.682)	0.086 (1.160)	0.192 (2.338)	0.218 (2.337)	0.257 (1.712)
Adductors	0.101	0.038	0.133	0.127	0.645
Abductors	0.155	0.076	0.141	0.182	0.218
External rotators	0.319	0.110	0.372	0.511	0.382
Internal rotators	0.163	0.073	0.160	0.247	0.646
Extensors	0.320	0.083	0.321	0.518	0.740
Flexors	0.172	0.083	0.178	0.219	0.601

Table 6 (continued)

	Plane-of-elevation	Elevation angle	Shoulder rotation	Elbow flexion	Pronation supination
ARC					
Baseline	0.611 (2.719)	0.084 (1.070)	0.393 (1.117)	1.005 (3.179)	0.821 (3.076)
Adductors	0.538	0.043	0.349	0.793	0.146
Abductors	0.314	0.085	0.201	0.454	1.004
External rotators	0.695	0.070	0.543	1.082	0.255
Internal rotators	0.476	0.081	0.243	0.522	0.536
Extensors	0.436	0.031	0.283	0.669	0.174
Flexors	0.452	0.050	0.278	0.654	1.715
SL					
Baseline	0.416 (5.898)	0.065 (1.856)	0.231 (3.436)	0.876 (5.149)	0.417 (3.895)
Adductors	0.684	0.089	0.403	1.292	0.454
Abductors	0.480	0.065	0.266	0.929	1.004
External rotators	0.500	0.097	0.407	1.027	0.363
Internal rotators	1.929	0.802	0.910	0.924	0.616
Extensors	0.502	0.059	0.296	0.980	0.375
Flexors	0.801	0.233	0.833	1.480	0.947
DL					
Baseline	0.429 (2.818)	0.162 (1.596)	0.563 (1.636)	0.880 (4.033)	0.755 (2.722)
Adductors	0.409	0.171	0.470	0.875	0.614
Abductors	0.441	0.138	0.380	0.613	0.602
External rotators	0.413	0.179	0.795	0.884	0.210
Internal rotators	**3.045**	**3.271**	**2.923**	0.817	2.441
Extensors	0.412	0.164	0.397	0.822	0.577
Flexors	0.384	0.141	0.467	0.742	0.924

References

[1] Gellman, H., Sie, I., and Waters, R. L., 1988, "Late Complications of the Weight-Bearing Upper Extremity in the Paraplegic Patient," Clin. Orthop. Relat. Res., **233**, pp. 132–135.

[2] Bayley, J. C., Cochran, T. P., and Sledge, C. B., 1987, "The Weight-Bearing Shoulder. The Impingement Syndrome in Paraplegics," J. Bone Jt. Surg.-Am., **69**(5), pp. 676–678.

[3] Akbar, M., Balean, G., Brunner, M., Seyler, T. M., Bruckner, T., Munzinger, J., Grieser, T., Gerner, H. J., and Loew, M., 2010, "Prevalence of Rotator Cuff Tear in Paraplegic Patients Compared With Controls," J. Bone Jt. Surg., **92**(1), pp. 23–30.

[4] Boninger, M. L., Souza, A. L., Cooper, R. A., Fitzgerald, S. G., Koontz, A. M., and Fay, B. T., 2002, "Propulsion Patterns and Pushrim Biomechanics in Manual Wheelchair Propulsion," Arch. Phys. Med. Rehabil., **83**(5), pp. 718–723.

[5] Kwarciak, A. M., Turner, J. T., Guo, L., and Richter, W. M., 2012, "The Effects of Four Different Stroke Patterns on Manual Wheelchair Propulsion and Upper Limb Muscle Strain," Disabil. Rehabil. Assist. Technol., **7**(6), pp. 459–463.

[6] Qi, L., Wakeling, J., Grange, S., and Ferguson-Pell, M., 2014, "Patterns of Shoulder Muscle Coordination Vary Between Wheelchair Propulsion Techniques," IEEE Trans. Neural Syst. Rehabil. Eng., **22**(3), pp. 559–566.

[7] Shimada, S. D., Robertson, R. N., Bonninger, M. L., and Cooper, R. A., 1998, "Kinematic Characterization of Wheelchair Propulsion," J. Rehabil. Res. Dev., **35**(2), pp. 210–218.

[8] Paralyzed Veterans of America Consortium for Spinal Cord Medicine, P. V. of A. C. for S. C., 2005, "Preservation of Upper Limb Function Following Spinal Cord Injury: A Clinical Practice Guideline for Health-Care Professionals," J. Spinal Cord Med., **28**(5), pp. 434–470.

[9] Koontz, A. M., Roche, B. M., Collinger, J. L., Cooper, R. A., and Boninger, M. L., 2009, "Manual Wheelchair Propulsion Patterns on Natural Surfaces During Start-Up Propulsion," Arch. Phys. Med. Rehabil., **90**(11), pp. 1916–1923.

[10] Madansingh, S. I., Fortune, E., Morrow, M. M., Zhao, K. D., and Cloud-Biebl, B. A., 2020, "Comparing Supraspinatus to Acromion Proximity and Kinematics of the Shoulder and Thorax Between Manual Wheelchair Propulsion Styles: A Pilot Study," Clin. Biomech., **74**, pp. 42–50.

[11] Walford, S. L., Rankin, J. W., Mulroy, S. J., and Neptune, R. R., 2021, "The Relationship Between the Hand Pattern Used During Fast Wheelchair Propulsion and Shoulder Pain Development," J. Biomech., **116**, p. 110202.

[12] Korkmaz, N., Yardmc, G., and Ylmaz, B., 2021, "Temporo-Spatial Parameters, Shoulder Kinematics and Acute Tendon Changes in Four Different Stroke Patterns in Men Wheelchair Users With Spinal Cord Injury," PMR., **14**(8), pp. 939–948.

[13] Lin, H.-T., Su, F.-C., Wu, H.-W., and An, K.-N., 2004, "Muscle Forces Analysis in the Shoulder Mechanism During Wheelchair Propulsion," Proc. Inst. Mech. Eng., Part H, **218**(4), pp. 213–221.

[14] Rankin, J. W., Richter, W. M., and Neptune, R. R., 2011, "Individual Muscle Contributions to Push and Recovery Subtasks During Wheelchair Propulsion," J. Biomech., **44**(7), pp. 1246–1252.

[15] Steenbrink, F., de Groot, J. H., Veeger, H. E. J., van der Helm, F. C. T., and Rozing, P. M., 2009, "Glenohumeral Stability in Simulated Rotator Cuff Tears," J. Biomech., **42**(11), pp. 1740–1745.

[16] van Drongelen, S., Schlüssel, M., Arnet, U., and Veeger, D., 2013, "The Influence of Simulated Rotator Cuff Tears on the Risk for Impingement in Handbike and Handrim Wheelchair Propulsion," Clin. Biomech., **28**(5), pp. 495–501.

[17] Morrow, M. M. B., Kaufman, K. R., and An, K.-N., 2010, "Shoulder Model Validation and Joint Contact Forces During Wheelchair Activities," J. Biomech., **43**(13), pp. 2487–2492.

[18] Van Drongelen, S., Van Der Woude, L. H., Janssen, T. W., Angenot, E. L., Chadwick, E. K., and Veeger, D. J. H., 2005, "Mechanical Load on the Upper Extremity During Wheelchair Activities," Arch. Phys. Med. Rehabil., **86**(6), pp. 1214–1220.

[19] Slowik, J. S., Requejo, P. S., Mulroy, S. J., and Neptune, R. R., 2016, "The Influence of Wheelchair Propulsion Hand Pattern on Upper Extremity Muscle Power and Stress," J. Biomech., **49**(9), pp. 1554–1561.

[20] Leving, M. T., Vegter, R. J. K., de Vries, W. H. K., de Groot, S., and L. H. V. van der Woude, 2018, "Changes in Propulsion Technique and Shoulder Complex Loading Following Low-Intensity Wheelchair Practice in Novices," PLoS One, **13**(11), p. e0207291.

[21] van Drongelen, S., de Groot, S., Veeger, H. E. J., Angenot, E. L. D., Dallmeijer, A. J., Post, M. W. M., and van der Woude, L. H. V., 2006, "Upper Extremity Musculoskeletal Pain During and After Rehabilitation in Wheelchair-Using Persons With a Spinal Cord Injury," Spinal Cord, **44**(3), pp. 152–159.

[22] Wilbanks, S. R., and Bickel, C. S., 2016, "Scapular Stabilization and Muscle Strength in Manual Wheelchair Users With Spinal Cord Injury and Subacromial Impingement," Top. Spinal Cord Inj. Rehabil., **22**(1), pp. 60–70.

[23] Mulroy, S. J., Hatchett, P., Eberly, V. J., Haubert, L. L., Conners, S., and Requejo, P. S., 2015, "Shoulder Strength and Physical Activity Predictors of Shoulder Pain in People With Paraplegia From Spinal Injury: Prospective Cohort Study," Phys. Ther., **95**(7), pp. 1027–1038.

[24] Burnham, R. S., May, L., Nelson, E., Steadward, R., and Reid, D. C., 1993, "Shoulder Pain in Wheelchair Athletes," Am. J. Sports Med., **21**(2), pp. 238–242.

[25] Curtis, K. A., Drysdale, G. A., Lanza, R. D., Kolber, M., Vitolo, R. S., and West, R., 1999, "Shoulder Pain in Wheelchair Users With Tetraplegia and Paraplegia," Arch. Phys. Med. Rehabil., **80**(4), pp. 453–457.

[26] Mulroy, S. J., Winstein, C. J., Kulig, K., Beneck, G. J., Fowler, E. G., DeMuth, S. K., Sullivan, K. J., Brown, D. A., and Lane, C. J., for the Physical Therapy Clinical Research Network (PTClinResNet), 2011, "Secondary Mediation and Regression Analyses of the PTClinResNet Database: Determining Causal Relationships Among the International Classification of Functioning, Disability and Health Levels for Four Physical Therapy Intervention Trials," Phys. Ther., **91**(12), pp. 1766–1779.

[27] Slowik, J. S., McNitt-Gray, J. L., Requejo, P. S., Mulroy, S. J., and Neptune, R. R., 2016, "Compensatory Strategies During Manual Wheelchair Propulsion in Response to Weakness in Individual Muscle Groups: A Simulation Study," Clin. Biomech., **33**, pp. 34–41.

[28] Lighthall-Haubert, L., Requejo, P. S., Mulroy, S. J., Newsam, C. J., Bontrager, E., Gronley, J. K., and Perry, J., 2009, "Comparison of Shoulder Muscle Electromyographic Activity During Standard Manual Wheelchair and Push-Rim Activated Power Assisted Wheelchair Propulsion in Persons With Complete Tetraplegia," Arch. Phys. Med. Rehabil., **90**(11), pp. 1904–1915.

[29] Rao, S. S., Bontrager, E. L., Gronley, J. K., Newsam, C. J., and Perry, J., 1996, "Three-Dimensional Kinematics of Wheelchair Propulsion," IEEE Trans. Rehabil. Eng., **4**(3), pp. 152–160.

[30] Slowik, J. S., Requejo, P. S., Mulroy, S. J., and Neptune, R. R., 2015, "The Influence of Speed and Grade on Wheelchair Propulsion Hand Pattern," Clin. Biomech., **30**(9), pp. 927–932.

[31] Sangeux, M., and Polak, J., 2015, "A Simple Method to Choose the Most Representative Stride and Detect Outliers," Gait Posture, **41**(2), pp. 726–730.
[32] Saul, K. R., Hu, X., Goehler, C. M., Vidt, M. E., Daly, M., Velisar, A., and Murray, W. M., 2015, "Benchmarking of Dynamic Simulation Predictions in Two Software Platforms Using an Upper Limb Musculoskeletal Model," Comput. Methods Biomech. Biomed. Eng., **18**(13), pp. 1445–1458.
[33] McFarland, D. C., Mccain, E. M., Poppo, M. N., and Saul, K. R., 2019, "Spatial Dependency of Glenohumeral Joint Stability During Dynamic Unimanual and Bimanual Pushing and Pulling," ASME J. Biomech. Eng., **141**(5), p. 051006.
[34] de Groot, J. H., and Brand, R., 2001, "A Three-Dimensional Regression Model of the Shoulder Rhythm," Clin. Biomech., **16**(9), pp. 735–743.
[35] Wu, G., van der Helm, F. C. T., Veeger, H. E. J., Makhsous, M., Van Roy, P., Anglin, C., Nagels, J., et al., 2005, "ISB Recommendation on Definitions of Joint Coordinate Systems of Various Joints for the Reporting of Human Joint Motion—Part II: Shoulder, Elbow, Wrist and Hand," J. Biomech., **38**(5), pp. 981–992.
[36] Millard, M., Uchida, T., Seth, A., and Delp, S. L., 2013, "Flexing Computational Muscle: Modeling and Simulation of Musculotendon Dynamics," ASME J. Biomech. Eng., **135**(2), p. 021005.
[37] Sabick, M. B., Kotajarvi, B. R., and An, K.-N., 2004, "A New Method to Quantify Demand on the Upper Extremity During Manual Wheelchair Propulsion," Arch. Phys. Med. Rehabil., **85**(7), pp. 1151–1159.
[38] Guo, L.-Y., Su, F.-C., Wu, H.-W., and An, K.-N., 2003, "Mechanical Energy and Power Flow of the Upper Extremity in Manual Wheelchair Propulsion," Clin. Biomech., **18**(2), pp. 106–114.
[39] Delp, S. L., Anderson, F. C., Arnold, A. S., Loan, P., Habib, A., John, C. T., Guendelman, E., and Thelen, D. G., 2007, "OpenSim: Open-Source Software to Create and Analyze Dynamic Simulations of Movement," IEEE Trans. Biomed. Eng., **54**(11), pp. 1940–1950.
[40] Thelen, D. G., Anderson, F. C., and Delp, S. L., 2003, "Generating Dynamic Simulations of Movement Using Computed Muscle Control," J. Biomech., **36**(3), pp. 321–328.
[41] Thelen, D. G., and Anderson, F. C., 2006, "Using Computed Muscle Control to Generate Forward Dynamic Simulations of Human Walking From Experimental Data," J. Biomech., **39**(6), pp. 1107–1115.
[42] Requejo, P. S., Lee, S. E., Mulroy, S. J., Haubert, L. L., Bontrager, E. L., Gronley, J. K., and Perry, J., 2008, "Shoulder Muscular Demand During Lever-Activated vs Pushrim Wheelchair Propulsion in Persons With Spinal Cord Injury," J. Spinal Cord Med., **31**(5), pp. 568–577.
[43] Mulroy, S. J., Gronley, J. K., Newsam, C. J., and Perry, J., 1996, "Electromyographic Activity of Shoulder Muscles During Wheelchair Propulsion by Paraplegic Persons," Arch. Phys. Med. Rehabil., **77**(2), pp. 187–193.
[44] Gutierrez, D. D., Mulroy, S. J., Newsam, C. J., Gronley, J. K., and Perry, J., 2005, "Effect of Fore-Aft Seat Position on Shoulder Demands During Wheelchair Propulsion: Part 2. An Electromyographic Analysis," J. Spinal Cord Med., **28**(3), pp. 222–229.
[45] Gagnon, D. H., Roy, A., Gabison, S., Duclos, C., Verrier, M. C., and Nadeau, S., 2016, "Effects of Seated Postural Stability and Trunk and Upper Extremity Strength on Performance During Manual Wheelchair Propulsion Tests in Individuals With Spinal Cord Injury: An Exploratory Study," Rehabil. Res. Pract., **2016**, pp. 1–11.
[46] Van Drongelen, S., Van Der Woude, L. H., Janssen, T. W., Angenot, E. L., Chadwick, E. K., and Veeger, D. H., 2005, "Glenohumeral Contact Forces and Muscle Forces Evaluated in Wheelchair-Related Activities of Daily Living in Able-Bodied Subjects Versus Subjects With Paraplegia and Tetraplegia," Arch. Phys. Med. Rehabil., **86**(7), pp. 1434–1440.
[47] Holloway, C. S., Symonds, A., Suzuki, T., Gall, A., Smitham, P., and Taylor, S., 2015, "Linking Wheelchair Kinetics to Glenohumeral Joint Demand During Everyday Accessibility Activities," Proceedings of the Annual International Conference of the IEEE Engineering in Medicine and Biology Society, EMBS, Institute of Electrical and Electronics Engineers Inc., Milan, Italy, Aug. 25–29, pp. 2478–2481.
[48] Veeger, H. E. J., Rozendaal, L. A., and Van der Helm, F. C. T., 2002, "Load on the Shoulder in Low Intensity Wheelchair Propulsion," Clin. Biomech., **17**(3), pp. 211–218.
[49] Zajac, F. E., Neptune, R. R., and Kautz, S. A., 2002, "Biomechanics and Muscle Coordination of Human Walking: Part I: Introduction to Concepts, Power Transfer, Dynamics and Simulations," Gait Posture, **16**(3), pp. 215–232.
[50] Yu, J., Ackland, D. C., and Pandy, M. G., 2011, "Shoulder Muscle Function Depends on Elbow Joint Position: An Illustration of Dynamic Coupling in the Upper Limb," J. Biomech., **44**(10), pp. 1859–1868.
[51] Labriola, J. E., Lee, T. Q., Debski, R. E., and McMahon, P. J., 2005, "Stability and Instability of the Glenohumeral Joint: The Role of Shoulder Muscles," J. Shoulder Elbow Surg., **14**(1), pp. S32–S38.
[52] Lippitt, S. B., Vanderhooft, J. E., Harris, S. L., Sidles, J. A., Harryman, D. T., and Matsen, F. A., 1993, "Glenohumeral Stability From Concavity-Compression: A Quantitative Analysis," J. Shoulder Elbow Surg., **2**(1), pp. 27–35.
[53] Ackland, D. C., and Pandy, M. G., 2009, "Lines of Action and Stabilizing Potential of the Shoulder Musculature," J. Anat., **215**(2), pp. 184–197.
[54] Mulroy, S. J., Newsam, C. J., Gutierrez, D. D., Requejo, P., Gronley, J. K., Haubert, L. L., and Perry, J., 2005, "Effect of Fore-Aft Seat Position on Shoulder Demands During Wheelchair Propulsion: Part 1. A Kinetic Analysis," J. Spinal Cord Med., **28**(3), pp. 214–221.
[55] Yanagawa, T., Goodwin, C. J., Shelburne, K. B., Giphart, J. E., Torry, M. R., and Pandy, M. G., 2008, "Contributions of the Individual Muscles of the Shoulder to Glenohumeral Joint Stability During Abduction," ASME J. Biomech. Eng., **130**(2), p. 021024.
[56] Belli, I., Joshi, S., Prendergast, J. M., Beck, I., Della Santina, C., Peternel, L., and Seth, A., 2023, "Does Enforcing Glenohumeral Joint Stability Matter? A New Rapid Muscle Redundancy Solver Highlights the Importance of Non-Superficial Shoulder Muscles," PLoS One, **18**(11), p. e0295003.
[57] Kumar, V. P., Satku, K., and Balasubramaniam, P., 1989, "The Role of the Long Head of Biceps Brachii in the Stabilization of the Head of the Humerus," Clin. Orthop. Relat. Res., **244**, pp. 172–175.